Supplementary material

S1. Comparison of observed data with isoGSM simulations and ERA5 reanalysis data

To effectively evaluate the applicability of isoGSM and examine the degree to which simulation results reproduce actual isotope effects, Fig. S1 presented four sets of correlation scatters between simulated and observed precipitation $\delta^{18}O_P$, $\delta^{18}O_P$ and *P*, $\delta^{18}O_P$ and *T*, and $\delta^{18}O_P$ and $\delta^{2}H_P$ at Changsha station. Statistics showed that the root mean square error between simulated and observed $\delta^{18}O_P$ was only 2.41‰, and the correlation coefficient between the two reached 0.53, far exceeding the 0.001 significance level (Fig. S1a). In seasonal variation, the observed and simulated average maximum $\delta^{18}O_P$ usually occurred in March-April, not in the month with minimum precipitation. The average minimum $\delta^{18}O_P$ usually occurred in July-September, not in the month with maximum precipitation (Fig. 2a; Main text). This indicated that the seasonal variation of precipitation isotopes in the monsoon region represented by Changsha did not correspond to the climate pattern of concurrent rainfall and heat.

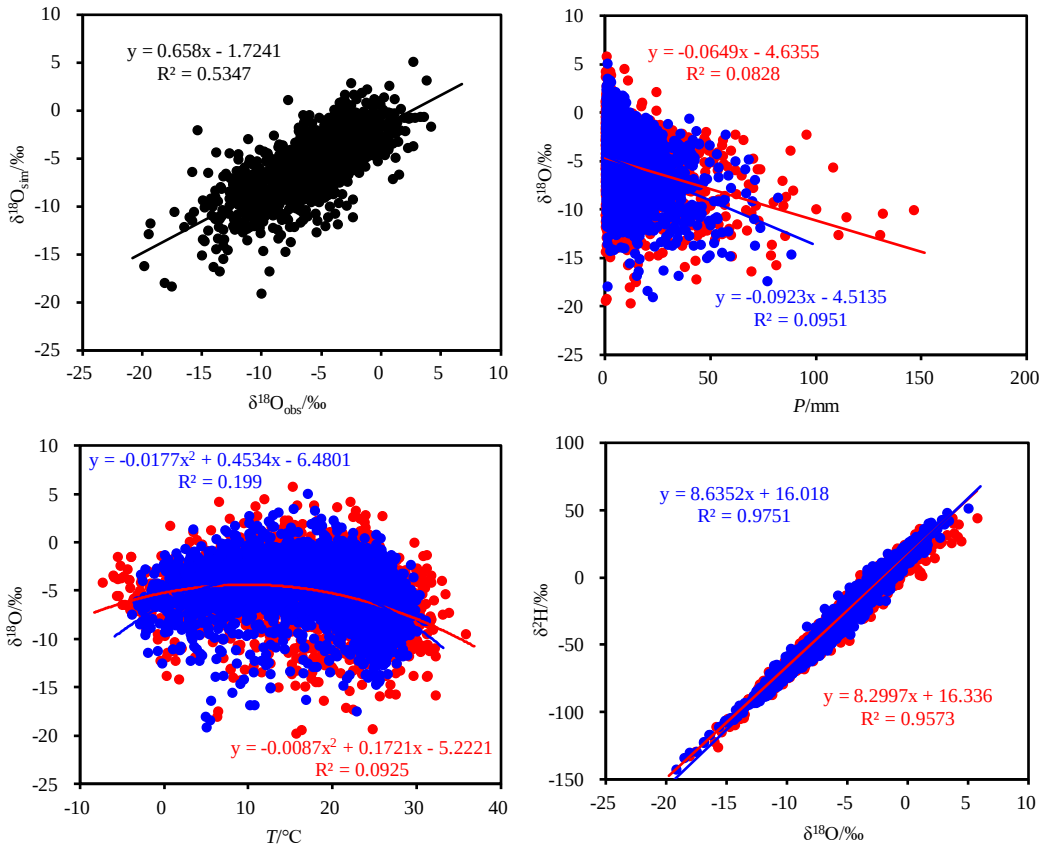

Fig. S1 Correlation scatters of observed and isoGSM-simulated (or by ERA5) $\delta^{18}O_P$ (a), $\delta^{18}O_P$ and P (b), $\delta^{18}O_P$ and T (c), and $\delta^{18}O_P$ and $\delta^{2}H_P$ (d) at Changsha station.

Observed daily P ranged from 0.1 to 146.4 mm (Fig. 2a; Main text). Among these, 568 days with P greater than the daily average of 11.0 mm accounted for 31.07% of total precipitation days, with a multi-year daily weighted average $\delta^{18}O_P$ of −7.22‰ corresponding to relatively large precipitation. The remaining 1260 days with P less than or equal to the average accounted for 68.93% of total precipitation days, with a daily weighted average $\delta^{18}O_P$ of −5.18‰ corresponding to relatively small P. The P from ERA5 at the corresponding grid point ranged from 0.1 to 88.3 mm. Among these, days with P greater than the multi-year daily average of 9.1 mm accounted for 34.11% of total precipitation days, with a daily weighted average $\delta^{18}O_P$ of −6.92‰. Days with $P \leq 9.1$ mm accounted for 65.99% of total precipitation days, with a daily weighted average $\delta^{18}O_P$ of −5.01‰. According to Fig. S1b, the simulated data accurately reproduced the P effect existing at Changsha station. Both the regression coefficient representing the rainout level and the intercept representing the average $\delta^{18}O$ of initial condensation in clouds, as well as the correlation coefficient representing the degree

of similarity, were very close between simulated and observed results.

Observed daily average T ranged from −7.3 to 35.9°C (Fig. 2a; Main text). Among these, 947 days with T greater than the daily average of 15.7°C accounted for 51.81% of total precipitation days, with a daily weighted average $\delta^{18}O_P$ of −7.41‰ and average P of 14.0 mm. The remaining 881 days with $T \leq 15.7$°C accounted for 48.19% of total precipitation days, with a daily weighted average $\delta^{18}O_P$ of −5.46‰ and average daily P of 7.8 mm. Daily average T from ERA5 ranged from −3.9 to 31.1°C. Days with T greater than the daily average of 18.5°C accounted for 57.82% of total precipitation days, with a daily weighted average $\delta^{18}O_P$ of −6.94‰ and average P of 10.9 mm. Days with $T \leq 18.5$°C accounted for 42.18% of total precipitation days, with a daily weighted average $\delta^{18}O_P$ of −5.23‰ and average P of 6.5 mm. Both observed and simulated results showed that the relationship between $\delta^{18}O_P$ and T was neither positively nor negatively correlated, but parabolic (Fig. S1c). This may be due to the seasonal distribution of precipitation isotopes in the study region, which were enriched in spring and depleted in summer and autumn (Fig. 2a; Main text).

According to the comparison in Fig. S1d, although isoGSM well reproduced the observed Local Meteoric Water Line (LMWL), with slopes greater than 8.0 and intercepts greater than 10.0‰ for the monsoon region being simulated, the model still slightly overestimated the influence of supersaturated environments in clouds (Zhang et al., 2016). In Changsha, June was the peak period of the summer monsoon and the month with the largest precipitation throughout the year, with the observed average P, T, and weighted average $\delta^{18}O_P$ of 207.7 mm, 24.4°C, and −8.40‰, respectively. The values for the average P, T, and weighted average $\delta^{18}O_P$ from ERA5 or isoGSM were 364.5 mm, 25.1°C, and −7.25‰, respectively. Moreover, January was the prevailing period of the winter monsoon, with observed average P, T, and weighted average $\delta^{18}O_P$ of 65.6 mm, 3.8°C, and −6.17‰, respectively. The values for the average P, T, and weighted average $\delta^{18}O_P$ from ERA5 or isoGSM were 74.6 mm, 5.3°C, and −6.29‰, respectively. The average meteorological characteristics and average precipitation isotopic characteristics of the representative months were well captured.

S2. Characteristics of wind direction and water vapor transport at different heights and locations relative to the front

According to classical meteorological theory (Zhou et al., 1997), in a cold front system, the wind blows from the southwest ahead of the front and from the northwest or northeast behind the front (Fig. S2a). Warm and moist air from low latitudes rises along the frontal surface to form precipitation, while cold air from high latitudes moves southward below the frontal surface, lifting the warm and moist air. At different heights and locations, air parcel movement directions and water vapor transport directions differ (Fig. S2b). For example, at Point A locate above the frontal surface on the warm and moist air side, air parcels and water vapor are both transported by southwest winds; at Point C locate below the frontal surface on the cold and dry air side, air parcels and water vapor are both transported by northwest or northeast winds; at Point B locate in the frontal zone, wind direction and speed are uncertain.

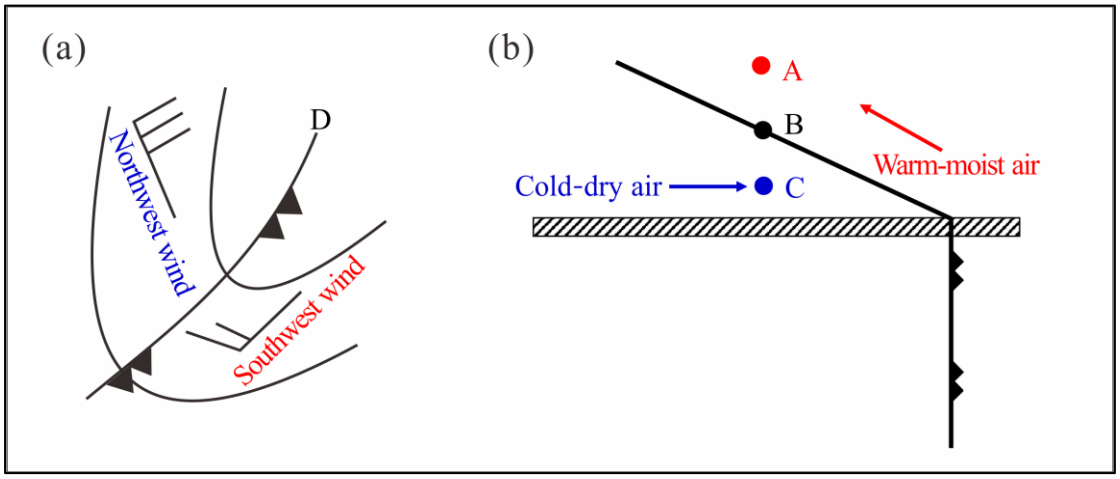

Fig. S2 Schematic diagram of cold front system in East Asia (based on Zhou et al., 1997).

References:

Zhou, S. Z. 1997. Meteorology and Climatology (in Chinese). Beijing: Higher Education Press, 118–222.